An empirical ocean color algorithm for estimating the contribution of chromophoric dissolved organic matter to total light absorption in optically complex waters

Simon Belanger, Marcel Babin, Pierre Larouche

An empirical ocean color algorithm for estimating the contribution of chromophoric dissolved organic matter to total light absorption in optically complex waters

Simon Bélanger,[1,2] Marcel Babin,[1] and Pierre Larouche[3]

Received 6 July 2007; revised 1 October 2007; accepted 16 November 2007; published 24 April 2008.

[1] To estimate the depth-integrated rate of photochemical processes involving chromophoric dissolved organic matter (CDOM) in coastal waters, the contribution of CDOM to the total absorption coefficient must be known from UV to green. At 307 sites sampled in various coastal marine environments, the ratio between CDOM and the total absorption coefficient ($[a_{CDOM}/a_t]$) at 412 nm was found to vary over a wide range, from 0.20 to 0.95. An empirical algorithm was developed to retrieve $[a_{CDOM}/a_t](412)$ from satellite remote sensing reflectance. The absolute uncertainty on the $[a_{CDOM}/a_t]$ retrieval was 0.14. As exemplified with the data from the Baltic and North Seas, the algorithm provides a means to distinguish the contribution of CDOM to the absorption coefficient of colored detrital material (i.e., CDM = CDOM + nonalgal particles) at the regional scale. The implications of the variability in the magnitude and spectral shape of $[a_{CDOM}/a_t]$ for the assessment of depth-integrated production of any photoproducts involving CDOM photolysis are discussed in details. We applied the algorithm to a Sea-viewing Wide Field-of-View Sensor (SeaWiFS) image of the Southeastern Beaufort Sea where terrestrial inputs are abundant. The spatial variability in the $[a_{CDOM}/a_t]$ reaches as much as threefold over the continental shelf and beyond. These results clearly show that it is necessary to account for the spatial variability of $[a_{CDOM}/a_t]$ when quantifying CDOM-related photochemical processes in the ocean.

Citation: Bélanger, S., M. Babin, and P. Larouche (2008), An empirical ocean color algorithm for estimating the contribution of chromophoric dissolved organic matter to total light absorption in optically complex waters, *J. Geophys. Res.*, *113*, C04027, doi:10.1029/2007JC004436.

1. Introduction

[2] Chromophoric dissolved organic matter (CDOM), operationally defined using the absorption coefficient (a_{CDOM}, in m^{-1}) of the material that passes through a 0.2 μm filter [*Nelson and Siegel*, 2002], is the major ultraviolet light (UVB and UVA; 280−320 and 320−400 nm respectively) absorber within most of the global ocean surface, except in ultraoligotrophic subtropical gyres waters [*Morel et al.*, 2007; *Nelson et al.*, 2007]. CDOM can also absorb a significant fraction of the visible light (400−700 nm) in the marine environment [*Bricaud et al.*, 1981], thus depressing the water-leaving radiance recorded by remote sensing sensors [*Carder et al.*, 1991].

[3] The knowledge of the actual proportion of the spectral light absorbed by CDOM, phytoplankton or nonalgal particles is desirable for many reasons including studies dealing with photochemical reactions. For example, in coastal waters where terrestrial inputs are important, CDOM can absorb up to 90% of the blue solar radiation (400−500 nm) [*Babin et al.*, 2003b; *Del Vecchio and Subramaniam*, 2004], hence competing with phytoplankton for photosynthetically active radiation (PAR) [*Keith et al.*, 2002; *McKee et al.*, 2002]. High concentration of detrital particulate matter can, on the other hand, shade the CDOM and phytoplankton from destructive UV light radiations. Besides, radiant energy absorbed by CDOM triggers numerous photochemical reactions that are of great importance for the carbon and nutrients cycles, and the air-sea exchanges of trace gases in the marine environment (see review by *Mopper and Keiber* [2002]). To quantify these reactions, one should know the contribution of CDOM to total light absorption in order to estimate the amount of radiant energy available for photochemical processes [e.g., *Zafiriou et al.*, 2003]. This is particularly important for the estimation of depth-integrated production of any of the photoproducts resulting from the CDOM photooxidation. The focus of the present study is the estimation of the contribution of CDOM to total light absorption, i.e., the ratio of a_{CDOM} to the total absorption coefficient ($[a_{CDOM}/a_t]$), from satellite ocean color remote sensing. Because a large variability in $[a_{CDOM}/$

[1]Laboratoire d'Océanographie de Villefranche, Centre National de la Recherche Scientifique, Université Pierre et Marie Curie, Villefranche-sur-Mer, France.
[2]Now at Département de Biologie, Chimie et Géographie, Université du Québec à Rimouski, Rimouski, Quebec, Canada.
[3]Institut Maurice-Lamontagne, Pêches et Océans Canada, Mont-Joli, Quebec, Canada.

0148-0227/08/2007JC004436

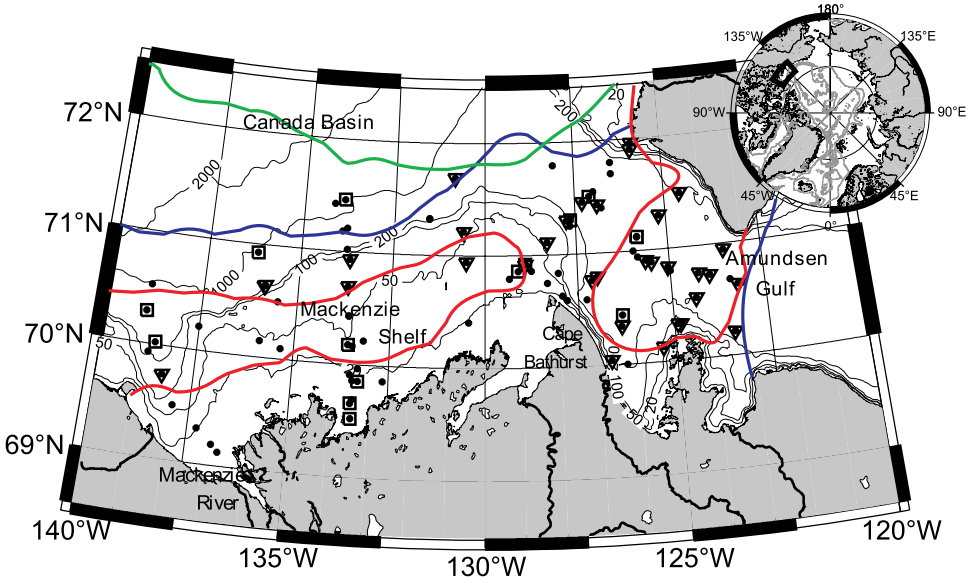

Figure 1. Map of the study area showing the location of stations where IOPs (dots), SPMR (triangles), and ASD (squares) measurements were made. Contour lines of sea ice concentration of 50% are also shown for 1 June (red), 1 July (blue), and 1 August (green).

a_t] is expected in coastal waters influenced by terrestrial input, our approach was developed mainly for waters defined as "Case 2" by *Morel and Prieur* [1977].

[4] During the last 2 decades, several semianalytical algorithms have been proposed to derive inherent optical properties (IOP) from the remote sensing reflectance spectrum [*Lee*, 2006]. None of these semianalytical approaches, however, are specifically designed to derive separately the total and CDOM absorption coefficients. Indeed, because CDOM and nonalgal particles (NAP) are characterized by similar exponentially decreasing absorption spectrum with increasing wavelength [*Bricaud et al.*, 1981; *Roesler et al.*, 1989], current algorithms fail to distinguish them and, as a practical solution, they combine them into a unique absorption coefficient referred to as colored detrital material (CDM = CDOM+NAP [see *Siegel et al.*, 2002]). While CDM is dominated by CDOM at the global scale (82 ± 14% at 440 nm according to *Siegel et al.* [2002]), the relative contribution of CDOM to CDM varies within a wide range in coastal waters (see below). Therefore our work was motivated by the lack of appropriate method to distinguish CDOM from the CDM, or to estimate the ratio [a_{CDOM}/a_t], in optically complex waters.

[5] Our first objective was to document the variability in the ratio [a_{CDOM}/a_t]. Using an extensive data set covering various coastal environments, we observed that [a_{CDOM}/a_t] at 412 nm varies between 0.20 to 0.94, with an average of 0.55 and a standard deviation (σ) of 0.15, which demonstrates the significance of the variability in [a_{CDOM}/a_t] in optically complex waters. The second objective was to propose an empirical algorithm for the retrieval of [a_{CDOM}/a_t] at 412 nm from the remote sensing reflectance spectrum. In what follows, we first present the in situ data sets used to develop our empirical algorithm. Next we discuss (1) the accuracy of the retrieved [a_{CDOM}/a_t](412) with the empirical coefficients derived from our in situ data set, and from other data sets, and (2) the implications of the variability in the spectral [a_{CDOM}/a_t] ratio for the depth-integrated estimation of any photoproducts involved in CDOM photochemistry (section 3.3). Finally, using Sea-viewing Wide Field-of-view Sensor (SeaWiFS) data, we illustrate the benefit of the proposed method for the quantification of photochemical processes in the Southeastern Beaufort Sea (section 3.4).

2. Materials and Methods

2.1. Data Sets Description and Measurements

[6] Two different data sets collected in various coastal environments are used in this study: the Coastal Surveillance Through Observation of Ocean Color (COAST/OOC) and the Canadian Arctic Shelf Exchange Study (CASES) data sets. Details on the time period and sampling locations of COAST/OOC is given by *Babin et al.* [2003a, 2003b]. Only the COAST/OOC data collected in coastal (so-called Case 2) waters were retained for the algorithm development and validation: 29 stations in the northern Adriatic Sea; 53 stations in the southwestern Baltic Sea; 68 stations in the North Sea; and 58 stations in the English Channel along the southern coast of England. CASES sampling was conducted in June and July 2004 onboard the CCGS *Amundsen* in the southeastern Beaufort Sea (Figure 1). The Amundsen Gulf was first sampled after the sea ice opening in June and was revisited in late July when most of the area was free of ice. The surface waters were, therefore, influenced by melt-waters at few stations. The Mackenzie Shelf was sampled during late June and early July when the Mackenzie River discharge peaks [*Macdonald et al.*, 1998], making those stations typical Case 2 waters. At 47 stations, our whole set of in situ optical measurements was achieved, while at other stations only IOP measurements (52 and 25 spectra of the particle and CDOM absorption coefficients, respectively) were made because of either sun elevation too high for proper apparent optical properties (AOP) measurements

(sun zenith angle >70°) or occasional technical problems with instruments (Figure 1).

2.1.1. Inherent Optical Properties

[7] Details on the IOP measurements for COAST/OOC are given by *Babin et al.* [2003a, 2003b]. Similar protocols were adopted during CASES with few modifications as described below. At each station, a sample of ~20 L of surface water was collected with a clean bucket for spectrophotometric analyses. Subsamples for the determination of a_{CDOM} were filtered through 0.2-μm Anotop® syringe filters (Whatman) and kept into 100-mL acid-cleaned amber glass bottles. For the determination of the absorption coefficient of particles, a_p, suspended particles were retained onto 25-mm GF/F glass fiber filters (Whatman®) by filtering 0.1 to 3.5 L of seawater. The glass bottles and GF/F filters were stored frozen (seawater: −20°C; particle: −80°C) in the dark until being analyzed two to four months later in the land based laboratory. Samples treatment and methods applied to determine the a_p and a_{CDOM} spectra are detailed by *Bélanger et al.* [2006] (see notation section). Briefly, $a_p(\lambda)$ was determined at 1-nm resolution between 350 and 750 nm according to the transmittance-reflectance protocol developed by *Tassan and Ferrari* [1995, 2002]. The measurements were stopped at 350 nm owing to the sharp decrease in the signal-to-noise ratio resulting from the high absorption by the GF/F filters below that wavelength, and the possible artifact in $a_p(\lambda)$ introduced by the possible presence of mycosporine-like amino acids [*Sosik*, 1999; *Laurion et al.*, 2003]. The $a_p(\lambda)$ values for $\lambda < 350$ were obtained by extrapolation using an exponential function fitted to the data between 350 and 360 nm (same as equation (1)). After a_p measurements, the filters were soaked during ~30 minutes in 90% methanol to extract phytoplankton pigments [*Kishino et al.*, 1985], and the transmittance-reflectance measurements were repeated for the determination of nonalgal absorption (a_{NAP}). The absorption coefficient of phytoplankton (a_ϕ) was assumed equal to $a_p(\lambda) - a_{NAP}(\lambda)$. The $a_{CDOM}(\lambda)$ was measured in 10-cm quartz cuvettes between 250 and 800 nm with 1-nm increments using a dual beam spectrophotometer (Perkin-Elmer Lambda 35). A background correction was applied by subtracting the absorbance value averaged over an interval of 5 nm around 685 nm from all the spectral values [*Babin et al.*, 2003b]. Then, the following model was fitted to the data between 300 and 500 nm using a nonlinear regression method (Levenberg-Marquardt):

$$a_{CDOM}(\lambda) = a_{CDOM}(\lambda_0)e^{S(\lambda_0-\lambda)}, \quad (1)$$

where λ_0 is a reference wavelength (here 443 nm) and S is the spectral slope of the $a_{CDOM}(\lambda)$ spectrum.

[8] The spectral absorption and beam attenuation coefficients of seawater constituents (i.e., excluding pure seawater itself), a_{t-w} and c_{t-w}, were determined at nine wavelengths (412, 440, 488, 510, 532, 555, 650, 676 and 715 nm) using a submersible spectrophotometer (ac-9, WET Labs Inc.). The ac-9 was either operated in the shipborne laboratory where ~20 L of surface water were passed through the instrument by gravity, or deployed from the deck or from a zodiac to obtain vertical profiles from surface down to ~40 m. The manufacturer calibration was checked daily using ~10 L of water purified onboard (Milli-Q Gradient A10, filtered with a Millipore RiOs 8). Temperature and salinity corrections were applied using the latest coefficients determined by the manufacturer. The ac-9 overestimates absorption coefficients owing to the loss of scattered photons within the reflecting tube before they reach the detector [*Zaneveld et al.*, 1994]. To correct for that error, the following expression was applied:

$$a_{t-w}(\lambda) = a_m(\lambda) - \varepsilon b_m(\lambda), \quad (2)$$

where $a_m(\lambda)$ is the measured absorption coefficient, $b_m(\lambda)$ is the measured scattering coefficient calculated as the difference $c_{t-w}(\lambda) - a_m(\lambda)$, and ε is the fraction of the scattering coefficient that corresponds to photons not detected by the sensor. We used the matrix inversion procedure proposed by *Gallegos and Neale* [2002] to estimate ε. The spectral shapes for $a_{CDOM}(\lambda)$, $a_{NAP}(\lambda)$ and $a_\phi(\lambda)$, and the relationship between $a_{NAP}(440)$ and $b_m(440)$, which are necessary in the inversion, were determined using measurements on discrete water samples (described above) following the statistically augmented method described by *Gallegos and Neale* [2002]. When available, the vertical $a_{t-w}(\lambda)$ profiles were optically averaged from surface down to the first attenuation length using the weighting function approach proposed by *Gordon* [1992].

[9] The ratio $[a_{CDOM}/a_t](412)$ was computed using the spectrophotometrically determined IOPs, except for seven of the CASES stations where $a_{CDOM}(412)$ was not available and was computed as $a_{t-w}(412) - a_p(412)$. A comparison of the two methods indicates that the $[a_{CDOM}/a_t](412)$ agree within ±0.11 at 95% confidence level.

2.1.2. Remote Sensing Reflectance

[10] During COAST/OOC, irradiance measurements were achieved from helicopter (202) and from ship (6). Vertical profiles of the spectral upwelling irradiance, $E_u(z, \lambda)$, and the spectral downwelling irradiance just above the sea surface, $E_s(0^+, \lambda)$, were measured at 13 wavebands (412, 443, 456, 490, 510, 532, 560, 620, 665, 683, 705, 779 and 866 nm) with a Satlantic free-fall SPMR (SeaWiFS Profiling Multichannel Radiometer) and SMSR (SeaWiFS Multichannel Surface Reference), respectively. Both radiometers had been calibrated less than 3 months before each cruise by the instrument manufacturer. Platform (ship or helicopter) shadow was avoided and, in the specific case of helicopter, instruments were deployed from an altitude high enough to avoid perturbation at sea surface created by the rotor air flux. After excluding data with an instrument tilt > 5°, the in-water profiles start beyond ~2 m when the radiometer was deployed in free-falling mode from a ship, and beyond ~0.2 m when deployed from a helicopter using a winch. To estimate upward irradiance just below the sea surface (at 0- m), $E_u(z, \lambda)$ profiles were extrapolated up to surface by fitting an exponential function to the data. The spectral remote sensing reflectance is calculated as

$$R_{rs}(\lambda) = 0.543\left(\frac{L_u(0^-,\lambda)}{E_s(0^+,\lambda)}\right)$$
$$L_u(0^-,\lambda) = \frac{E_u(0^-,\lambda)}{Q}, \quad (3)$$

where 0.543 is a factor for propagating the radiance through the air-sea interface [*Mueller et al.*, 2003] and Q (units sr) is a factor that relates any in-water upwelling radiance to the in-water upwelling irradiance. Here a Q value of 3.8 was used, which falls within the range calculated for turbid coastal waters [*Loisel and Morel*, 2001].

[11] During CASES, the remote sensing reflectance at 13 wavebands (405, 412, 434, 442, 490, 510, 520, 532, 555, 590, 665, 683 and 700 nm), $R_{rs}(\lambda)$, was calculated from the vertical profile of $L_u(z, \lambda)$, and $E_s(0^+, \lambda)$ measured with a SPMR and SMSR, respectively. At each station, three to five SPMR casts were performed at least 50 m away from the ship to avoid ship shadow. The upwelling radiances were extrapolated to the subsurface, $L_u(0\text{-}, \lambda)$, using a linear fit to all $\ln[L_u(z, \lambda)]$ data points measured within a depth interval of 2−3 m that start beyond ∼2−3 m. Note that the relative difference between $L_u(0\text{-}, \lambda)$ obtained with a linear fit and the one obtained by fitting an exponential function was <1%. For each station, we averaged $R_{rs}(\lambda)$ obtained from different casts (2 to 4) after elimination of the spectra different from the mean value by more than 10% in the blue. Out of 40 stations with SPMR measurements, 34 $R_{rs}(\lambda)$ were retained for the algorithm development (section 2.2). Note that four spectra were eliminated because the difference among all replicates was >10%, and two because the surface waters stratification was such that appropriate extrapolation could not be achieved.

[12] Note that both measured $E_u(0^-, \lambda)$ and $L_u(0^-, \lambda)$ were corrected for instrument self-shading following the method proposed by *Gordon and Ding* [1992] as applied by *Zibordi and Ferrari* [1995] using $a_{t-w}(\lambda)$ measurements made with the ac-9 and the $a_w(\lambda)$ values published by *Pope and Fry* [1997].

[13] In shallow water areas or when surface waters were stratified (i.e., 13 stations), the $R_{rs}(\lambda)$ was measured above the sea surface using a hyperspectral radiometer (336 to 1062 nm with $\Delta\lambda$ = 1.42 nm; Analytical Spectral Device, ASD). To make measurements away from the ship shadow and bubble clouds, the instrument was mounted at the end of the ship bow and deployed either on the port or starboard side depending of the sun position and the sea state. As for in-water measurements, only data obtained when incident irradiance conditions were stable (clear or uniformly cloudy skies) were retained. To avoid calibration issues that generally result from the use of multiple sensors, the measurements of the radiance (acceptance angle of 10°) coming from sea surface (L_t), downwelling sky (L_{sky}), and a Lambertian reflector (grey Spectralon) (L_p) were performed successively, within a few minutes, using a unique sensor. To obtain one R_{rs} spectrum, five to ten scans of each quantity were quality checked and averaged. Note that the ASD automatically adjusts the integration time of the measurements to optimize the signal-to-noise ratio (1.09 to 4.35 s for L_t, and <1 s for L_{sky} and L_p). The above-water remote sensing reflectance is calculated as [*Mobley*, 1999]

$$R_{rs}(\lambda) = \frac{\left(L_t(\lambda) - \rho_{sky} \cdot L_{sky}(\lambda)\right) \cdot R_p}{\pi L_p(\lambda)}, \tag{4}$$

where ρ_{sky} is the air-water interface specular reflection coefficient for radiance, and R_p is the albedo of the lambertian panel (88.3%). The value of R_p, spectrally constant in the visible and near infrared parts of the spectrum, was determined using a calibrated lambertian panel (P. Minnett, U. of Miami; calibration performed on 4 May 2004 by Avian Technologies LLC inc.). As recommended by *Mobley* [1999], L_t was measured with a viewing zenith angle of ∼40° and a relative azimuth angle of ∼135°. For clear sky condition, published ρ_{sky} values by *Mobley* [1999] was used (his Figure 9), which varies as a function of the in situ measured wind speed and the solar zenith angle. For cloudy sky condition, a value 0.0256 was adopted for ρ_{sky} [*Mobley*, 1999]. An additional spectrally neutral correction was applied to $R_{rs}(\lambda)$ on the basis of the known spectral shape of R_{rs} in the near infrared (NIR) part of the spectrum [*Ruddick et al.*, 2006]. This procedure aims to correct the R_{rs} spectra for uncertainty due to the air-sea reflection correction (for details see web appendix 2 of *Ruddick et al.* [2006]). The correction assumes that the ratio of water leaving reflectance between two wavelengths in the NIR is constant and known (here 780 and 870 nm were used), allowing the computation of a residual error that is then subtracted from $R_{rs}(\lambda)$. Except for two relatively turbid stations in the estuary ($R_{rs}(780) > 0.001$), all other stations felt within the range where the similarity spectrum assumption in the NIR is valid [*Ruddick et al.*, 2006]. This correction method improves the results particularly under cloudy condition when $\rho_{sky}L_{sky}$ is high relative to L_t, probably owing to the uncertainty on ρ_{sky} under these conditions.

2.2. Description of the $[a_{CDOM}/a_t]$ Algorithm

[14] To improve the quantification of photooxidation, one needs to know the spectral contribution of a_{CDOM} to the total light absorption coefficient of seawater. As mentioned in the Introduction, because of the similar spectral absorption spectra of CDOM and NAP, semianalytical algorithms currently found in the literature fail to discriminate them. Here we propose an empirical method to obtain the ratio $[a_{CDOM}/a_t]$ at 412 nm, directly from the R_{rs} spectrum. The $[a_{CDOM}/a_t](412)$ was regressed against several combinations of $R_{rs}(\lambda)$ and ratios of $R_{rs}(\lambda)$ selected according to the following rationales (or assumptions): in coastal waters, (1) reflectance at 412 nm is the most affected by CDOM absorption compared with other channels, (2) reflectance at 490 nm is the most affected by phytoplankton absorption, (3) variations in reflectance at 555 nm is mostly driven by light scattering by particles, and (4) a major distinctive property of CDOM is that it does not contribute to particle scattering. These considerations led us to propose the following empirical algorithm for the retrieval of $[a_{CDOM}/a_t]$, based on multiple regression conducted using measured $[a_{CDOM}/a_t](412)$ and $R_{rs}(\lambda)$,

$$\left[\frac{a_{CDOM}}{a_t}\right](412) = \alpha + \beta \cdot \log_{10}\left(\frac{R_{rs}(412)}{R_{rs}(555)}\right) + \chi \cdot \log_{10}\left(\frac{R_{rs}(490)}{R_{rs}(555)}\right) + \delta \cdot \log_{10}\left(R_{rs}(555)\right), \tag{5}$$

where α, β, χ and δ are empirical coefficients. When CDOM increases, for instance, the ratio $R_{rs}(412)/R_{rs}(555)$ decreases

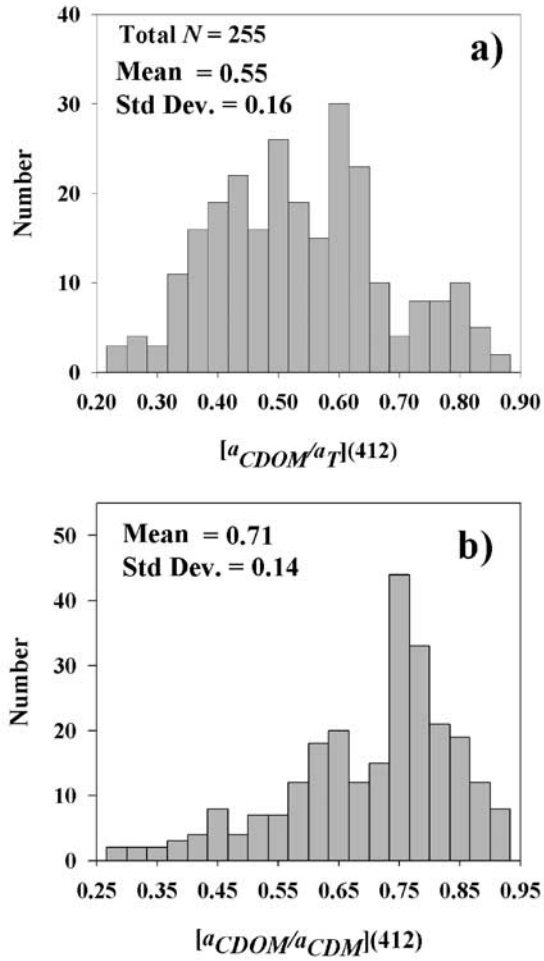

Figure 2. Frequency distributions of the contribution of CDOM to (a) the total light absorption at 412 nm ($[a_{CDOM}/a_t]$) and (b) the colored detrital material ($[a_{CDOM}/a_{CDM}]$).

and $[a_{CDOM}/a_t](412)$ tends to increase (negative slope for β). In contrast, when phytoplankton pigments increase, the ratio $R_{rs}(490)/R_{rs}(555)$ decreases and $[a_{CDOM}/a_t](412)$ tends to decrease (positive slope for χ). Finally, when the total amount of suspended particles increases, $R_{rs}(555)$ increases and $[a_{CDOM}/a_t](412)$ tends to decrease (negative slope for δ).

3. Results and Discussion

3.1. Variability of $[a_{CDOM}/a_t]$ and $[a_{CDOM}/a_{CDM}]$ in Coastal Waters

[15] Figure 2a illustrates the observed variability of $[a_{CDOM}/a_t]$ in the violet part of the spectrum in various coastal environments including the Adriatic Sea, Baltic Sea, English Channel, North Sea, and Beaufort Sea. Overall, $[a_{CDOM}/a_t]$ at 412 nm varies between 0.20 and 0.94, with an average of 0.55 and a standard deviation (σ) of 0.15, which confirms the large variability of $[a_{CDOM}/a_t](412)$ in coastal waters. The frequency distribution is slightly flat compared with a normal distribution (negative kurtosis). The range reported here is similar to the one observed in the western tropical North Atlantic Ocean where Amazon River inputs are important [*Del Vecchio and Subramaniam*, 2004].

[16] The contribution of CDOM to the total detrital material (CDM) also varies over a wide range in coastal waters, from 0.26 to 0.95 (Figure 2b and Table 1), even at regional scale (e.g., North Sea, 0.26 to 0.91). On average, $[a_{CDOM}/a_{CDM}]$ at 412 nm was 0.71 with a σ of 0.14. For comparison, *Siegel et al.* [2002] reported a mean value for the ratio $[a_{CDOM}/a_{CDM}]$ of 0.82 with a σ of 0.13 from a global collection of in situ absorption measurements of a_{CDOM} and a_{NAP}. Note that these values were reported at 440 nm by *Siegel et al.* [2002], which is lower than the expected values at 412 nm owing to the steeper slope for CDOM relative to NAP spectra. This is significantly higher than most values found in coastal waters influenced by river runoff or sediment resuspension [e.g., *Del Vecchio and Subramaniam*, 2004]. Therefore, the use of semianalytical ocean color models that retrieve $a_{CDM}(440)$ [*Lee*, 2006] are of limited utility for quantifying CDOM photooxidation in coastal waters.

3.2. Retrieval of $[a_{CDOM}/a_t]$ From Remote Sensing Reflectance

[17] Table 2 provides the multiple regression results for the empirical coefficients of equation (5) and the determination coefficients (R^2) obtained for the whole data set (generic optically complex waters algorithm, hereafter denoted as generic OCW algorithm), and separately for the five different regions of the data set (region-specific OCW algorithms). Figure 3 compares the $[a_{CDOM}/a_t]$ at 412 nm retrieved using the generic OCW algorithm with the measured values.

[18] To evaluate rigorously the ability of our algorithm to retrieve $[a_{CDOM}/a_t](412)$ in a given region, we conducted a cross validation exercise: the empirical coefficients of equation (5) for a given region were derived using the data from the four other regions. The algorithm could thereby be tested with a data set different from that used for algorithm tuning. For the Beaufort Sea, for example, the coefficients of equation (5) were derived using the whole COAST/OOC data set (i.e., Adriatic Sea, Baltic Sea, English Channel and North Sea). Note that these coefficients are not provided as they were derived for validation purpose only. Table 3

Table 1. Relative Contribution of CDOM to the Colored Detrital Matter (CDM = CDOM + NAP) and to the Total Absorption Coefficients at 412 nm, for the Different Regions Covered by Our Data Set

		$[a_{CDOM}/a_{CDM}](412)$			$[a_{CDOM}/a_t](412)$		
Area	N	Minimum	Maximum	Average ± σ	Minimum	Maximum	Average ± σ
Adriatic	29	0.38	0.87	0.63 ± 0.12	0.22	0.66	0.40 ± 0.09
Baltic	53	0.60	0.84	0.76 ± 0.05	0.38	0.72	0.60 ± 0.06
English Channel	58	0.30	0.91	0.72 ± 0.13	0.24	0.69	0.50 ± 0.10
North Sea	68	0.26	0.91	0.61 ± 0.16	0.20	0.81	0.49 ± 0.13
Beaufort Sea	47	0.41	0.95	0.82 ± 0.13	0.39	0.94	0.75 ± .13
All	255	0.26	0.95	0.71 ± 0.14	0.20	0.94	0.55 ± 0.15

Table 2. Empirical Coefficients of Equation (5) Determined by Multiple Regression for the Different Coastal Environments

Area	N	α	β	χ	δ	R^2
Adriatic	29	−0.015	−0.321	0.691	−0.223	0.46
Baltic	53	0.078	−0.133	0.674	−0.280	0.81
English Channel	58	−0.048	−0.423	0.539	−0.204	0.33
North Sea	68	−0.480	−0.255	0.526	−0.483	0.65
Beaufort Sea	47	−0.514	−0.546	0.480	−0.454	0.42
All	255	−0.387	−0.387	0.577	−0.390	0.70

provides the results from a comparison between retrieved and measured $[a_{CDOM}/a_t]$ for each region as obtained using Type-II regression. The algorithm captures part of the variability within each region as the regression slopes are all significantly positive, ($p < 0.05$), although they are significantly < 1 ($p < 0.05$), except for the English Channel. This result indicates that further tuning is necessary to get the variability of $[a_{CDOM}/a_t](412)$ right within a given region. Nevertheless, the overall absolute uncertainty of the algorithm with the coefficient derived independently is ±0.18 at the 95% confidence interval (Table 3). Despite the relatively high heterogeneity among the five coastal areas considered here, the algorithm is able to retrieve the average $[a_{CDOM}/a_t](412)$ value for each region (the mean absolute difference between the retrieved and measured $[a_{CDOM}/a_t]$ at 412 nm, $\overline{\Delta[a_{CDOM}/a_t]} = \pm 0.039$), except for the Beaufort Sea where the estimation is slightly biased ($\overline{\Delta[a_{CDOM}/a_t]} = -0.078$).

[19] In an attempt to understand the above results, we further analyzed the absolute difference between the retrieved and measured $[a_{CDOM}/a_t](412)$ values ($\Delta[a_{CDOM}/a_t]$). Again for each region, $[a_{CDOM}/a_t](412)$ was retrieved using equation (5) with the coefficients derived independently. Figure 4a compares $\Delta[a_{CDOM}/a_t]$ with the ratio between the particulate absorption at 412 nm and the remote sensing reflectance at 555 nm ($[a_p(412)/R_{rs}(555)]$), for each station. A positive $\Delta[a_{CDOM}/a_t]$ value indicates an overestimation of $[a_{CDOM}/a_t](412)$ by the empirical algorithm, and vice versa. Low values of the ratio $[a_p(412)/R_{rs}(555)]$ suggest that the particles are weakly absorbing blue photons relative to the their scattering properties in the green, while high values indicate the contrary. The former may result from the presence of mineral particles, and the latter the presence of phytoplankton and/or detritus [e.g., *Gallegos and Neale*, 2002]. Since the absolute value of $R_{rs}(555)$ is used in the algorithm as an indicator of the total amount of particles, variability in the $[a_p(412)/R_{rs}(555)]$ will affect the performance of the algorithm. Statistically significant positive slopes of the regression (Type II) between $\Delta[a_{CDOM}/a_t]$ and the logarithm of $[a_p(412)/R_{rs}(555)]$ were observed in the Adriatic Sea, Baltic Sea, English Channel and the North Sea (Table 4). These results suggest that the $[a_{CDOM}/a_t](412)$ value is, as argued above, underestimated in presence of weakly absorbing particles, while it is overestimated in presence of highly absorbing ones. This is because the enhancement of $R_{rs}(555)$ in presence of weakly absorbing particles results, for instance, in an overestimation of the contribution of particles to the total light absorption at 412 nm. But one may wonder why in the Baltic Sea, where particles are predominantly organic (e.g., 87% from *Babin et al.* [2003a]) and highly absorbing (Figure 4a), the $[a_{CDOM}/a_t](412)$ is not systematically overestimated? The answer can be found in Figure 4b.

[20] Figure 4b plots the absolute difference between the retrieved and measured $[a_{CDOM}/a_t](412)$ values ($\Delta[a_{CDOM}/a_t]$), as a function of the ratio between a_{CDOM} to a_{CDM} at 412 nm. Low values (< 0.5) of the ratio $[a_{CDOM}/a_{CDM}](412)$ indicate that NAP dominates the yellow substances (i.e., $a_{CDOM} + a_{NAP}$). In the algorithm, the ratio $R_{rs}(412)/R_{rs}(555)$ is used as an indicator of a_{CDOM} but the presence of NAP also affect this ratio. In other words, $R_{rs}(412)/R_{rs}(555)$ is an indicator of the total yellow substances rather than just the CDOM. The use of the absolute value of $R_{rs}(555)$ should compensate for the ambiguity between CDOM and NAP. Nevertheless it is expected that when the NAP dominates the CDM, the empirical algorithm will tend to slightly overestimate $[a_{CDOM}/a_t](412)$. Indeed statistically significant negative slopes of the linear regression (Type II) between $\Delta[a_{CDOM}/a_t]$ and $[a_{CDOM}/a_{CDM}](412)$ were observed in the Adriatic Sea, Baltic Sea, North Sea and Beaufort Sea (Table 4). Altogether, the R^2 of the regression reaches 0.21. The fact that relatively high $[a_{CDOM}/a_{CDM}](412)$ is found in the Baltic Sea partly explains why we do not observe a systematic overestimation of $[a_{CDOM}/a_t](412)$ as expected on the basis of the previous observations (see previous paragraph). In the Beaufort Sea, the systematic underestimation of $[a_{CDOM}/a_t](412)$ by the empirical algorithm (−0.078; Table 3) is probably due to the dominance of CDOM in CDM ($[a_{CDOM}/a_{CDM}](412) = 0.82 \pm 0.13$).

[21] The biases described above weaken, or disappear, when the algorithm is tuned with the region-specific data. Figure 5 compares the retrieved and measured $[a_{CDOM}/a_t](412)$ values when the coefficients of equation (5) are derived for each region individually (Table 2). The regional tuning improves the correlation between retrieved and measured values (R^2 of 0.78 compared to 0.70), but there is still significant scatter around the 1:1 line (Figure 3 versus Figure 5). For the Baltic Sea and North Sea, the regional tuning leads

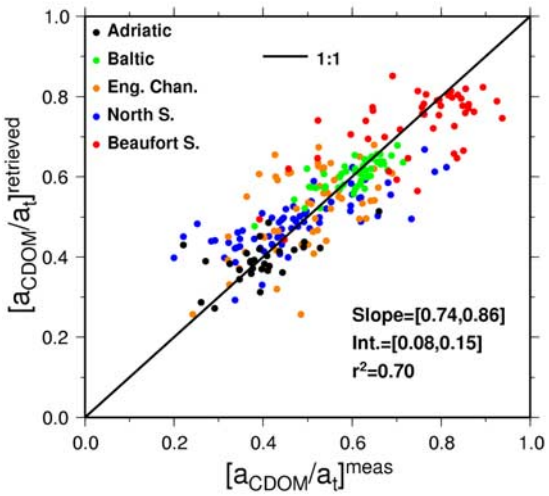

Figure 3. Comparison between retrieved and measured $[a_{CDOM}/a_t]$ at 412 nm for the COAST/OOC and CASES data sets. The $[a_{CDOM}/a_t](412)$ was calculated using equation (5) with coefficients obtained for the whole data set (generic OCW algorithm) ($N = 255$; Table 2).

Table 3. Results of a Type II Regression Between Retrieved and Measured $[a_{CDOM}/a_t]$ at 412 nm Using Equation (5)[a]

Area	N	Intercept[b]	Slope[b]	$\overline{\Delta[a_{CDOM}/a_t]}$[c]	$CI^{95\%}$[d]
Adriatic	29	0.22 [0.11, 0.31]	0.44 [0.21, 0.71]	0.001	±0.13
Baltic	53	0.28 [0.20, 0.34]	0.54 [0.43, 0.67]	0.000	±0.07
English Channel	58	0.00 [−0.30, 0.17]	1.06 [0.69, 1.64]	0.039	±0.20
North Sea	68	0.27 [0.22, 0.32]	0.45 [0.36, 0.54]	0.013	±0.17
Beaufort Sea	47	0.30 [0.13, 0.46]	0.56 [0.36, 0.80]	−0.078	±0.20
All	255	0.16 [0.12, 0.20]	0.70 [0.63, 0.76]	−0.002	±0.18

[a]For each region, an independent data set is used to obtain the empirical coefficients for equation (5).
[b]Numbers in brackets are for the range of 95% Confidence Interval computed for a Type II regression.
[c]$\overline{\Delta[a_{CDOM}/a_t]} = \frac{1}{N}\sum_{1}^{N}[a_{CDOM}/a_t]^{retrieved} - [a_{CDOM}/a_t]^{measured}$.
[d]The 95% confidence interval of the $[a_{CDOM}/a_t]$ retrieval.

to $R^2 > 0.65$. In the North Sea, in particular, where the composition of CDM is highly variable ($[a_{CDOM}/a_{CDM}](412) = 0.26$ to 0.91; Table 1), the algorithm is able to retrieve the ratio $[a_{CDOM}/a_t]$ within a $CI^{95\%}$ of 0.13 (Table 5). In the Baltic Sea, where the optical properties of particles are relatively homogeneous (Figure 4), the algorithm performance is excellent ($R^2 = 0.81$, $CI^{95\%} = \pm 0.05$). For the English Channel, in contrast, the algorithm poorly performs as indicated by the low R^2 of 0.33. For the Adriatic Sea and Beaufort Sea, because most of the measured $[a_{CDOM}/a_t](412)$ values felt within a narrow range, it is difficult to draw clear conclusions from this analysis. The overall absolute uncertainty of the region-specific OCW algorithms is ±0.14 at the 95% confidence interval.

[22] Our results suggest that an algorithm based on the ratios $R_{rs}(412)/R_{rs}(555)$ and $R_{rs}(490)/R_{rs}(555)$, and on $R_{rs}(555)$ is suitable to discriminate a_{CDOM} from a_t at 412 nm with good accuracy. We also applied this combination to the synthetic data set developed by the International Ocean Color Coordinating Group to test and compare algorithms (available at: http://www.ioccg.org/groups/OCAG_data.html). The performance of the algorithm was similar to that found with our in situ data set ($R^2 = 0.65$, $CI^{95\%} \pm 0.15$), but the β and χ coefficients of equation (5) were quite different (−.385, −1.105, 1.33 and −.342 for α, β, χ and δ respectively). Applying these coefficients to optically complex waters may result in unrealistically high values > 0.95 compared with our field observations (see Table 1 and auxiliary material[1]). The difference between coefficients values may be ascribed to the wide range of IOPs covered by the synthetic data set, and in particular to the highly variable ratio between the scattering and absorption coefficients of NAP (more than 1 order of magnitude). In addition, the synthetic data set includes clear waters for which the pure water absorption is no longer negligible at 412 nm (up to 33% of a_t). This fourth optically active component complicates the estimation of $[a_{CDOM}/a_t](412)$ with the coefficients derived for our OCW data set.

[23] Our method was also tested on the NASA bio-Optical Marine Algorithm Data set (NOMAD) [*Werdell and Bailey*, 2005]. The algorithm did not perform as well as on our in situ data set or on the IOCCG data set ($R^2 = 0.30$, $CI^{95\%} \pm 0.22$). Two possible explanations for this poor result are (1) the relatively low influence of terrestrial inputs in most of the NOMAD data set compare to our data set, and (2) the lack of consistency among the different sub-data sets that form the NOMAD data set, in terms of methods to measure the absorption coefficients adopted by different investigator. For some specific sub-data sets found in NOMAD, however, results similar to the one presented above were obtained. For example, $R^2 = 0.81$ and $CI^{95\%} \pm 0.14$ for the *ONR-Chesapeake* program, a region where similar

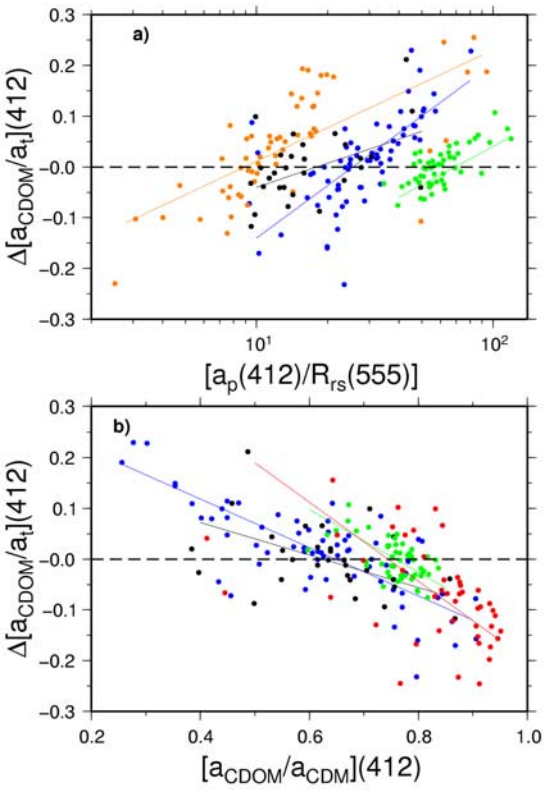

Figure 4. Plot of the absolute difference between the retrieved and measured $[a_{CDOM}/a_t]$ at 412 nm calculated using region-independent coefficients, as a function of (a) the ratio of $a_p(412)$ to $R_{rs}(555)$ and (b) the relative contribution of CDOM to the total CDM absorption coefficient at 412 nm. Only the statistically significant relationships are shown. Shading is the same as Figure 3.

[1]Auxiliary materials are available in the HTML. doi:10.1029/2007JC004436.

Table 4. Coefficients of Determination of the Linear Regression Between $\Delta[a_{CDOM}/a_t]$ (shown in Figure 4) and (1) the Logarithm of the Ratio $[a_p(412)/R_{rs}(555)]$ and (2) the Ratio $[a_{CDOM}/a_{CDM}]$ at 412 nm[a]

Area	N	$[a_p(412)/R_{rs}(555)]$[b]	$[a_{CDOM}/a_{CDM}](412)$[b]
Adriatic	29	**0.23** (NS)	0.18 (**0.17**)
Baltic	53	**0.51** (NS)	0.34 (NS)
English Channel	58	**0.46** (0.14)	NS (**0.23**)
North Sea	68	0.46 (**0.33**)	**0.58** (0.25)
Beaufort Sea	47	NS (0.21)	**0.22** (**0.27**)
All	255	0.15 (0.08)	**0.21 (0.14)**

[a]NS indicates that the slope of the regression was not significantly different from 0 ($p < 0.05$) (Type II regression).

[b]Values in parentheses are for the regionally tuned algorithm, while the bold numbers indicate the parameter that explains most the error for a given region.

variability was observed in terms of $[a_{CDOM}/a_t]$ and $[a_{CDOM}/a_{CDM}]$ [*Harding et al.*, 2005]. These results suggest that our algorithm works properly in coastal waters influenced by terrestrial inputs, and indicate that more data measured following unique protocols, for the absorption in particular, are necessary to validate such an algorithm.

[24] The application of equation (5) to SeaWiFS L_{wn} climatology has been successfully attempted. For a global application of our generic OCW algorithm, however, we recommend that an algorithm be first applied to distinguish optically complex from case-1 waters. For example, case-1 and case-2 pixels may be identified using the method proposed by *Lee and Hu* [2006], and then $[a_{CDOM}/a_t](412)$ may be calculated using the coefficients derived from the IOCCG (representing oceanic waters) and OCW data sets, respectively (see auxiliary material). Note, however, that even if the IOCCG data set was developed with the aim of representing the natural variability in IOPs as well as possible, it cannot be considered as an absolute reference for the tuning of an algorithm.

3.3. Implications of $[a_{CDOM}/a_t](\lambda)$ Variability for Depth-Integrated Photoproduction

[25] The use of ocean color data to calculate photochemical rates in the marine environment has been first proposed by *Cullen et al.* [1997]. Recently, *Johannessen et al.* [2003] modified Cullen et al.'s approach as following. First, the diffuse attenuation coefficient (K_d) at three UV bands (i.e., 323, 338 and 380 nm) is estimated using empirical relationships between the ratio $R_{rs}(412)/R_{rs}(555)$ and K_d(UV). Second, a_{CDOM} at 323, 338 and 380 nm is estimated assuming a constant ratio between a_{CDOM} and K_d at these wavelengths (i.e., 0.90, 0.86 and 0.97 respectively). The estimates of absorption and attenuation coefficients are then combined with surface irradiance to calculate the amount of radiant energy absorbed by the CDOM as a function of depth. As already pointed out by these authors, the ratio between a_{CDOM} and K_d may vary markedly in turbid waters because of the presence of other absorbing material (e.g., organic detritus), and/or significant particle scattering. This problem, i.e., the variations of the ratio a_{CDOM}/K_d or a_{CDOM}/a_t, is addressed in this section in terms of the quantitative assessment photochemical rates in optically complex environments. Specifically, our objectives here were to (1) study the impact of the variations of $[a_{CDOM}/a_t]$ on the depth-integrated production of dissolved inorganic carbon (P_{DIC}), a major photoproduct of CDOM photooxidation (see review by *Mopper and Keiber* [2002]), and (2) examine the uncertainties related to the spectral extrapolation of $[a_{CDOM}/a_t]$ derived at 412 nm from ocean color data.

[26] Quantitative assessment of CDOM photooxidation requires the knowledge of (1) the incident irradiance in the ultraviolet (UV) and visible parts of the spectrum, (2) the spectral contribution of CDOM to total light absorption, and (3) the spectral apparent quantum yield of the reaction (AQY). The latter is defined as the ratio of the number of photoproduct molecules formed per photon absorbed by the CDOM. The spectral photoproduction rate of any photoproducts involved in photochemical reactions, x (e.g., DIC), can be calculated as

$$P_x(\lambda) = E_d(0^-, \lambda)(1 - R(\lambda))\frac{a_{CDOM}(\lambda)}{a_t(\lambda)}AQY_x(\lambda), \quad (6a)$$

which can be integrated over the spectral range where photochemical reactions are efficient to obtain the depth-integrated value as

$$P_x = \int_{\lambda\min}^{\lambda\max} E_d(0^-, \lambda)(1 - R(\lambda))\frac{a_{CDOM}(\lambda)}{a_t(\lambda)}AQY_x(\lambda)d\lambda, \quad (6b)$$

where $\lambda_{\min}$ and $\lambda_{\max}$ are the limits of the integral (typically 280−300 and 450−600 nm, respectively), $R(\lambda)$ is the in-water irradiance reflectance (i.e., E_u/E_d), and $E_d(0^-, \lambda)$ is the spectral downward irradiance just beneath sea surface. Assuming that all photon that cross the air-sea interface are absorbed within the water column, the term $1 - R(\lambda)$ can be ignored. Typically $1 - R(\lambda)$ is equal to ~0.99 in spectral range considered here. Note that equation (6b) is an exact solution of the radiative transfer equation under the assumption that the water column is optically homogeneous.

[27] P_{DIC} was calculated using equation (6b) for 63 spectra of a_{CDOM}/a_t and two AQY spectra, while $E_d(0^-, \lambda)$ was kept constant (calculated using the Tropospheric Ultra-

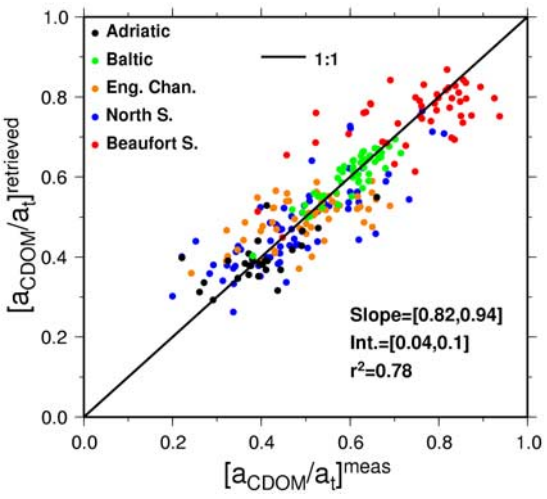

Figure 5. Same as Figure 3 but for region-specific coefficients in equation (5) (Table 2).

Table 5. Same as Table 3 but for Region Specific Coefficients in Equation (5)[a]

Area	N	Intercept	Slope	$\overline{\Delta[a_{CDOM}/a_t]}$	$CI^{95\%}$
Adriatic	29	0.17 [0.06, 0.26]	0.57 [0.21, 0.71]	0.000	±0.12
Baltic	53	0.07 [−0.01, 0.13]	0.89 [0.78, 1.02]	0.000	±0.05
English Channel	58	0.29 [0.21, 0.37]	0.41 [0.26, 0.58]	0.001	±0.16
North Sea	68	0.11 [0.04, 0.17]	0.77 [0.64, 0.91]	0.000	±0.13
Beaufort Sea	47	0.36 [0.21, 0.49]	0.52 [0.35, 0.72]	0.003	±0.19
All	255	0.07 [0.04, 0.10]	0.88 [0.82, 0.94]	0.000	±0.14

[a]See Table 2.

violet Visible (TUV) model [*Madronich and Flocke*, 1999] for the summer solstice, at latitude of 70°N, under clear sky, moderate aerosols concentration (optical thickness at 550 nm = 0.1), and total ozone column content of 330 DU). The two AQY spectra (AQY_1 and AQY_2) were determined in the southeastern Beaufort Sea by *Bélanger et al.* [2006] (Figure 6). The $[a_{CDOM}/a_t](\lambda)$ spectra were calculated using various values for $[a_{CDOM}/a_t](412)$ (0.2, 0.3, 0.4, 0.5, 0.6, 0.7, 0.9) and three different spectral shapes for both a_{CDOM} and a_p (see below) (Figure 7).

[28] The spectrally-depth-integrated DIC photoproduction between 300 to 500 nm (P_{DIC}; equation (6b)) was normalized to P_{DIC}^{max} which assumes $[a_{CDOM}/a_t](\lambda) = 1$ (examples of P_{DIC} (λ) are shown in Figure A1). Results of the calculations are illustrated in Figure 8. In the extreme case where $[a_{CDOM}/a_t](412) = 0.2$, the P_{DIC} would be overestimated by threefold if calculated using the assumption of $[a_{CDOM}/a_t](\lambda) = 1$. Figure 8 shows that P_{DIC} decreases almost linearly with the decrease in $[a_{CDOM}/a_t](412)$, while the slope of the different curves depends of the spectral extrapolation of $[a_{CDOM}/a_t](412)$. Briefly, this extrapolation is made assuming a wide range of spectral shape for both a_{CDOM} and a_p based on field observations in coastal waters (Figure 7). For a given value of $[a_{CDOM}/a_t](412)$, $[a_{CDOM}/a_t](\lambda)$ can be calculated if the spectral slope of CDOM spectrum is known, as well as the spectral shape of the total particulate absorption (see Appendix A for more details on the extrapolation procedure).

[29] The impact of the variation in the spectral shape of a_{CDOM} and a_p is relatively weak when CDOM dominates the total light absorption ($[a_{CDOM}/a_t](412) > 0.7$). This is particularly true for the AQY_2 as all curves are stacked down to a $[a_{CDOM}/a_t](412)$ value of 0.6 (Figure 8b). In contrast, uncertainties in P_{DIC} resulting from the extrapolation of $[a_{CDOM}/a_t](412)$ are relatively more important when particulate matter dominates the total light absorption (i.e., $[a_{CDOM}/a_t](412) < 0.6$). For example when $[a_{CDOM}/a_t](412) = 0.2$, P_{DIC}/P_{DIC}^{max} falls between 0.23 and 0.37 for AQY_1. P_{DIC} is more sensitive to the extrapolation when AQY_1 is used in the calculation. This is because the relative contribution of longer wavelengths is more impor-

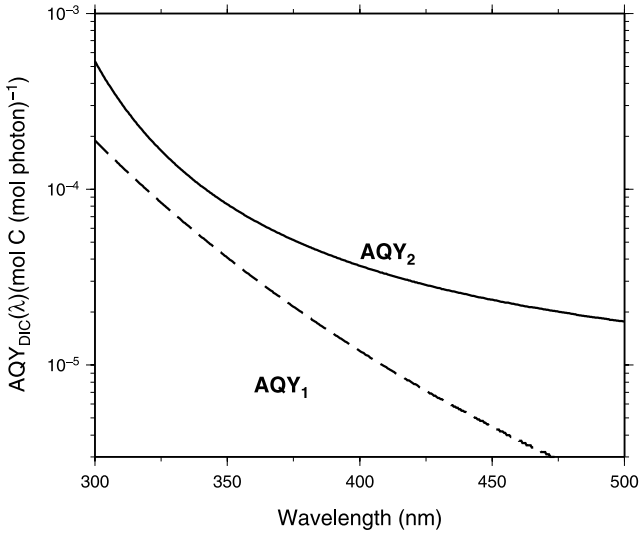

Figure 6. Apparent quantum yield spectra for DIC production determined for two stations located in the southeastern Beaufort Sea. AQY_2 was determined on surface waters influenced the by the Mackenzie River (salinity = 8.2 ‰; Station R5a), while AQY_1 was determined on surface waters collected in the Amundsen Gulf, away from direct riverine influence (salinity = 30.0 ‰; Station 108) [*Bélanger et al.*, 2006].

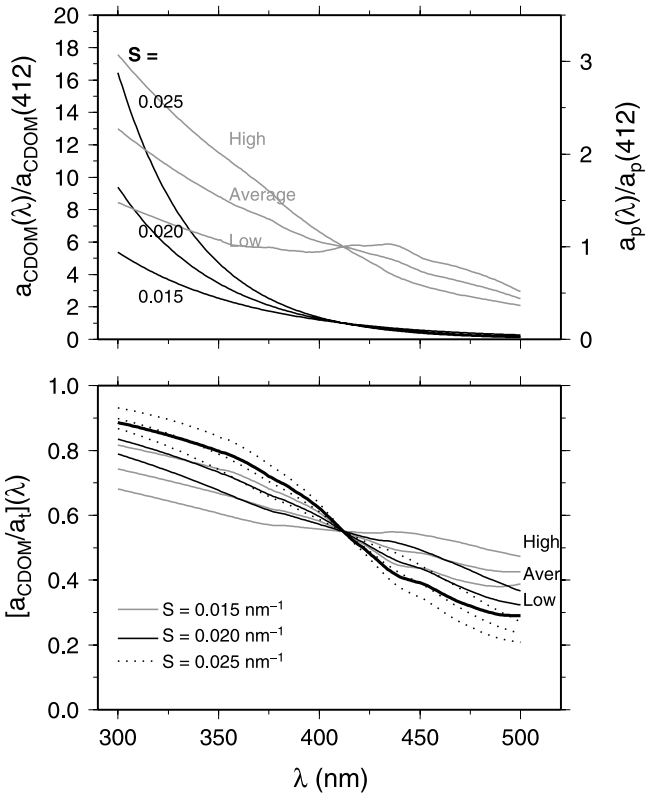

Figure 7. (top) Typical CDOM and particulate absorption spectra normalized to $a_{CDOM}(412)$ and $a_p(412)$, respectively. (bottom) Example of $[a_{CDOM}/a_t]$ spectra obtained (equation (A1)) when $[a_{CDOM}/a_t](412) = 0.5$ and all nine possible combinations of $a_{CDOM}(\lambda)$ and $a_p(\lambda)$ (see Appendix A).

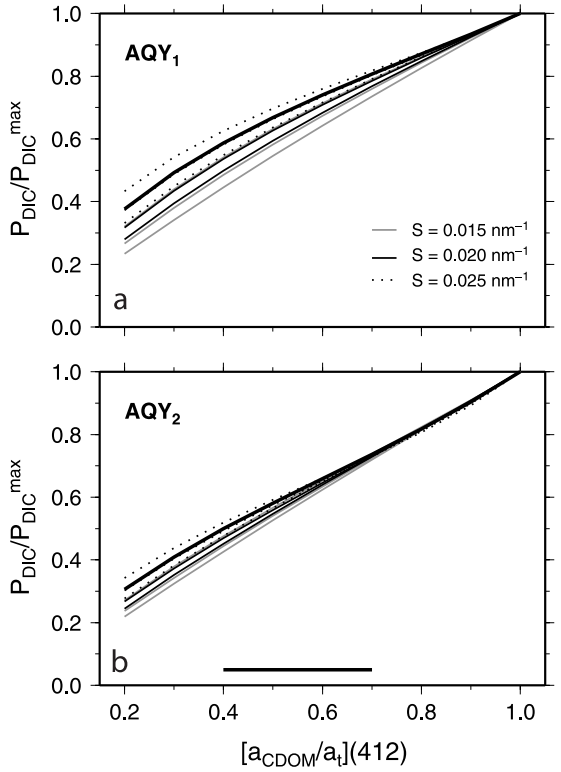

Figure 8. Variation of the depth-integrated P_{DIC} normalized to its value calculated using $[a_{CDOM}/a_t](\lambda) = 1$ as a function of $[a_{CDOM}/a_t](412)$. The thick horizontal line in Figure 8b indicates $[a_{CDOM}/a_t](412) = 0.55 \pm 0.15$ (mean $\pm$ σ). The different curves represents nine different $[a_{CDOM}/a_t](\lambda)$ spectra obtained by extrapolating $[a_{CDOM}/a_t](412)$ with various spectral shape for a_{CDOM} and a_p.

tant for AQY_1 than AQY_2 (Figure 6). For instance, a flat AQY (e.g., AQY_2) spectrum will tend to underestimate $P_{DIC}(\lambda)$ for $\lambda < 412$, which is compensated by an overestimation at $\lambda > 412$ (compare Figure A1c to Figure A1d).

[30] In general, if $[a_{CDOM}/a_t]$ at 412 nm is retrieved using remote sensing reflectance and extrapolated using averaged a_{CDOM} and a_p spectra, then P_x can be modeled within an error < 20% (of course if the AQY is known a priori). Nevertheless, these uncertainties are much lower than the actual variability in $[a_{CDOM}/a_t](412)$ (Table 1), which should be accounted for when estimating depth-integrated production of any photoproducts involved in the CDOM photochemistry.

[31] Note that the extrapolation of $[a_{CDOM}/a_t](412)$ to the whole spectral domain between 300 to 500 nm may be hazardous in some waters because of the presence of UV absorbing compound like MAAs, which are produced by several microorganisms living in the marine environment [*Morrison and Nelson*, 2004]. However, measurements of a_p in the UV domain is very uncertain with the current quantitative filter pad technique [*Laurion et al.*, 2003]. So the lack of reliable a_p measurements < 350 nm prevents the development of a more robust extrapolation method.

3.4. Application to SeaWiFS Imagery

[32] On a volume basis, the Arctic Ocean receives the highest amount of terrigenous dissolved organic carbon (DOC) relative to the world ocean [*Rachold et al.*, 2004]. During the past decade, dramatic changes have been observed in the Arctic ice climate, ocean circulation, storage of freshwater, ozone concentration, permafrost thawing and riverine discharge [*Arctic Climate Impact Assessment*, 2005]. Recently, *Bélanger et al.* [2006] have shown that CDOM photooxidation, in terms of depth-integrated photoproduction of DIC, in the southeastern Beaufort Sea (western Arctic) has increased over the last 25 years mostly in response to reducing ice cover. Because this region is influenced by the Mackenzie River, which annually supplies enormous amounts of runoff (330 km^3), suspended particles (124 Tg) and DOC (1.3 Tg) [*Macdonald et al.*, 1998], optical properties of the surface waters are largely controlled by terrigenous inputs. The spatial and temporal variability of the optical properties of the surface waters are, therefore, expected to be high during the spring-summer season when the photooxidation occurs and the river plume spreads over the continental shelf. The objective in this section is to estimate $[a_{CDOM}/a_t]$ from SeaWiFS imagery and to use it in the equation (6b) to calculated the DIC photoproduction in this area.

[33] We applied our algorithm to a full resolution SeaWiFS image of the southeastern Beaufort Sea acquired on 21 June 1998 (day 172). On that year, the sea ice cover was exceptionally reduced in early spring over the study area, which allowed good ocean color observations over the whole Mackenzie Shelf and a large portion of the Canada Basin. The application of a turbid-water detection algorithm [*Morel and Bélanger*, 2006] revealed that almost two thirds of the ice-free waters were turbid. Therefore, the scene was processed using the turbid-water atmospheric correction algorithm proposed by *Ruddick et al.* [2000]. The $[a_{CDOM}/a_t](412)$, calculated using equation (5) with region-specific coefficients (Table 2), shows coherent patterns over the continental shelf and beyond (Figure 9a). First, $[a_{CDOM}/a_t](412)$ values increase from the river mouth to the border of the continental shelf, from $\sim$0.4 to $\sim$0.9. This may reflect the decreasing contribution of the terrigenous particles to the total light absorption in the surface waters when the particles gradually settle over the continental shelf. This decrease in turbidity may be observed in the $L_{wn}(555)$ image (Figure 9b). For the whole image, the $[a_{CDOM}/a_t](412)$ and $L_{wn}(555)$ are inversely correlated ($r = -0.88$), which indicates that $[a_{CDOM}/a_t](412)$ increases as the turbidity decreases. However, the highest values (>0.9) are found beyond the continental shelf in waters influenced by the CDOM from the Mackenzie River, but less by terrigenous particles from this river, which are still present. Further offshore in the Canada Basin and in the Amundsen Gulf, while the turbidity is still decreasing (Figure 9b), the $[a_{CDOM}/a_t](412)$ decreases and reaches relatively uniform values ranging between 0.7 and 0.8. These lower offshore values probably reflect the absence of direct influence of river runoff and a relatively more important contribution of phytoplankton to total light absorption. The values observed there fall within the range that was observed in situ during CASES.

[34] Figure 10 shows the spatial distribution of the depth-integrated DIC photoproduction rate (in mg C m^{-2} d^{-1}) for both AQYs, as calculated using the satellite-derived $[a_{CDOM}/a_t](412)$ values (Figure 9). The spectral extrapolation of $[a_{CDOM}/a_t](412)$ was achieved using equation (A1) with the averaged S (i.e., 0.022 nm^{-1}) and $a_p^N(\lambda)$ (defined as

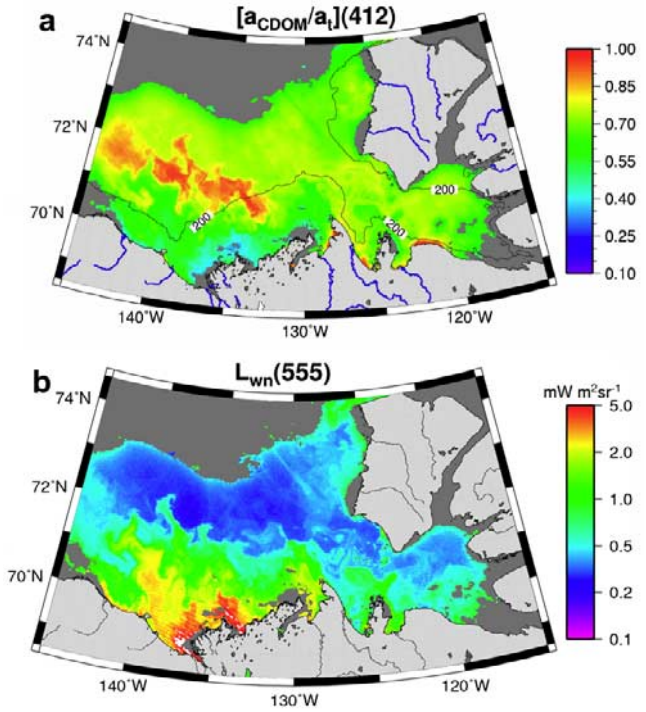

Figure 9. Spatial distribution of (a) the $[a_{CDOM}/a_t](412)$ and (b) the normalized water-leaving radiance at 555 nm, as derived from SeaWiFS data acquired on 21 June 1998. The grey color code represents sea ice.

$a_p^N(\lambda) = a_p(\lambda)/a_p$ (412), see Appendix A) measured in the Beaufort Sea [*Bélanger*, 2006]. The daily spectral irradiance just below the sea surface, $E_d(0^-,\lambda)$, was obtained using the TUV model with the spatially averaged ozone concentration derived from the total ozone mapping spectrometer (TOMS) data and optical thickness derived from SeaWiFS data ($E_d(0^-,\lambda)$ was assumed constant over the whole scene). The spatial distribution of the P_{DIC} is similar to that of $[a_{CDOM}/a_t](412)$ with the highest values of ~10−12 and ~3.6−3.8 mg C m^{-2} d^{-1} for AQY_2 and AQY_1, respectively, observed at the border of the continental shelf. The spatial variability in P_{DIC} is slightly higher for AQY_1 (~2.5-fold) than for AQY_2 (~2-fold). These results confirm that the spatial variability in P_{DIC} resulting from the optical properties of the water column alone is important. As shown by *Bélanger et al.* [2006], however, the variability in AQY may be much greater than that of optical properties.

4. Summary and Conclusions

[35] Depth-integrated production of any photoproducts involved in the CDOM photochemistry can be assess using a simple spectral model that needs as input, among other, the ratio between the CDOM and total absorption coefficients ($[a_{CDOM}/a_t]$). To account for the important variability of this ratio in coastal waters, an empirical algorithm was proposed to estimate the $[a_{CDOM}/a_t]$ ratio at 412 nm from the remote sensing reflectance spectrum. The algorithm was developed and validated using an extensive data set of in situ measurements of spectral absorption coefficients and reflectance made in contrasting optically complex waters. The absolute uncertainty of the algorithm was found to be ±0.18 (±0.14 for regional tuning). When the composition of particles is relatively stable, i.e., the amount of mineral versus organic matter is relatively constant, regional tuning of the algorithm can provide even more reliable estimates of $[a_{CDOM}/a_t](412)$ (e.g., uncertainty of ±0.055 in the Baltic Sea). The application of our approach to SeaWiFS imagery in the Southeastern Beaufort Sea demonstrates that variations in $[a_{CDOM}/a_t]$ have a significant impact on the spatial DIC photoproduction patterns in coastal waters.

[36] The empirical algorithm proposed in the present study, however, should only be used in optically complex waters for the following reasons. First, the empirical coefficients were derived using a relatively small data set obtained in coastal waters influenced by significant terrestrial input. Secondly, in the open ocean, there is significant absorption by pure water itself, which is not well represented with our data set. Recent findings by *Morel et al.* [2007, Table 1] suggest that pure water may largely dominate the total light absorption in the huge subtropical gyres of the Pacific Ocean even in the UVb domain (i.e., >50% at 310 nm). In other words, empirical coefficients for oceanic waters, based on measurements, are still needed to estimate the contribution of CDOM to the total light absorption at the global scale.

[37] One may wonder why an empirical algorithm succeeds in separating CDOM and NAP absorption, while current semianalytical algorithms do not. We believe that if it is possible with an empirical algorithm, which means that the information is contained in the reflectances, it must be possible with a semianalytical algorithm. We identified two aspects that need more attention for future semianalytical algorithms to be successful in discriminating a_{CDOM}

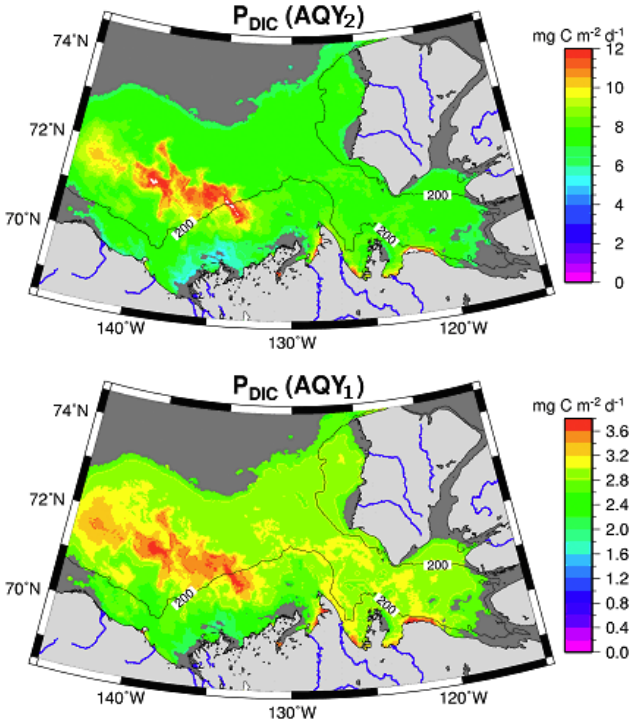

Figure 10. Spatial distribution of depth-integrated DIC photoproduction as calculated using two different AQYs and the satellite-derived $[a_{CDOM}/a_t](412)$ shown in Figure 9.

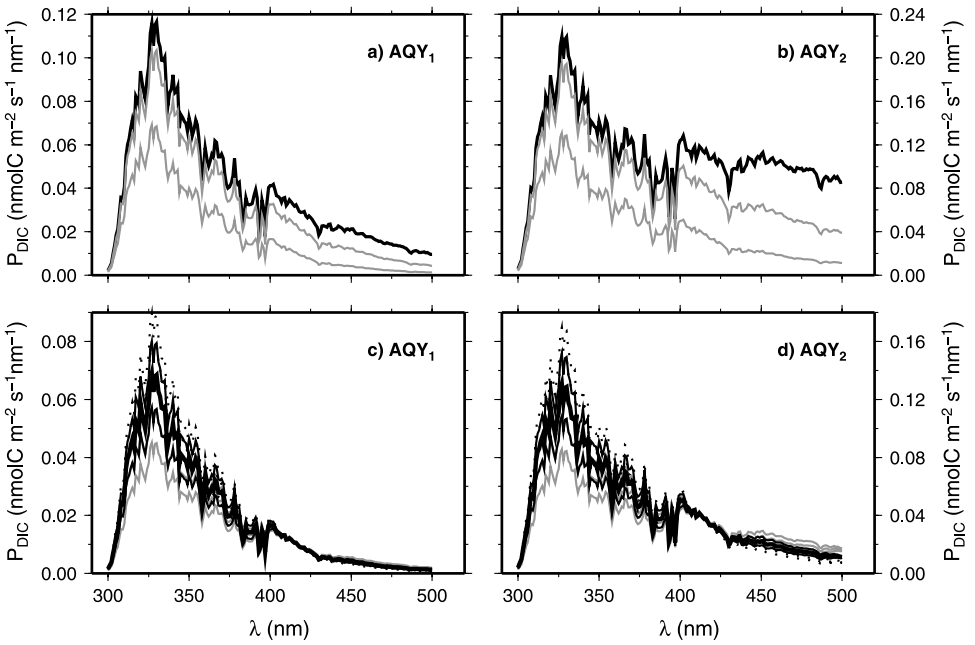

Figure A1. Examples of spectra P_{DIC} (equation (6a)) calculated with two AQYs and various $[a_{CDOM}/a_t](\lambda)$. (a, b) The $[a_{CDOM}/a_t](412) = 1$, 0.75, and 0.35, and the extrapolation was performed using $S = 0.020\ \text{nm}^{-1}$ and chl = 1.0 mg m^{-3}. (c, d) The $[a_{CDOM}/a_t](412) = 0.5$ and the extrapolation was performed for all possible combinations of $a_{CDOM}(\lambda)$ and $a_p(\lambda)$ (i.e., nine spectra).

from the total absorption coefficient in coastal waters: the IOP model formulation and the inversion approach.

[38] While the fact that NAP scatters light and CDOM does not is a source of ambiguity when pooling CDOM and NAP, it provides discrimination power when CDOM and NAP are distinguished in an IOP model. So, semianalytical algorithms need to be based on an IOP model that includes a good link between a_{NAP} and b_{NAP} (or b_{bNAP}). *Gallegos and Neale* [2002] successfully applied such an approach to deconvolve the absorption contribution by phytoplankton, CDOM and NAP in total absorption spectra measured in situ. But, obviously, the inversion of remotely sensed reflectance is more challenging than inverting absorption spectra measured in situ.

[39] Again, the fact that our empirical algorithm succeeded in discriminating a_{CDOM} from a_{NAP} means that the necessary information is contained in the reflectance spectrum. This information, however, must be extracted properly, and this is probably one weakness of current semianalytical models. In coastal waters, variations in reflectance are primarily due to variations in turbidity [*Sathyendranath et al.*, 1989]. Subtle changes in the shape of the reflectance spectrum that may result from changes in the proportions of phytoplankton, CDOM and NAP, are overwhelmed by the change in the magnitude of reflectance at all wavelengths due to variations in turbidity. So, when specific information is needed from the reflectance spectrum, such as the ratio of a_{CDOM} to a_t, some specific spectral regions provide less ambiguous information. The rationales considered in the development of our empirical algorithm are also valid for a semianalytical algorithm. The latter must go beyond finding the best fit between calculated and observed reflectance spectra, at all wavelengths [e.g., *Roesler and Perry*, 1995; *Lee et al.*, 1996; *Garver and Siegel*, 1997]. This procedure must not be blurred by the large changes in reflectance magnitude due to variations in turbidity, and be misled by reflectance at wavelengths where the information is ambiguous (see *Defoin-Platel and Chami* [2007] for a detailed analysis of the ambiguity problem in the interpretation of ocean color). Nevertheless, recent validation exercises have demonstrated the ability of semianalytical algorithms to retrieve the total absorption and backscattering coefficients. So, both approaches (i.e., semianalytical and empirical) may be combined to solve optical problems in optically complex waters.

[40] The simple method proposed in this study represents, to our knowledge, a first step toward the integration of Ocean Color information to quantify of CDOM-related photochemical processes in optically complex waters.

Appendix A

[41] Assuming that the pure water is negligible compare to nonwater absorption coefficients over the 300 to 500 nm range (i.e., $a_w(\lambda) = 0$), the spectral extrapolation of $[a_{CDOM}/a_t](412)$ can be achieve simply using assumed spectral shape for a_{CDOM} and a_p respectively. While $a_{CDOM}(\lambda)$ can be expressed using equation (1), an averaged a_p spectrum normalized to $a_p(412)$ is needed (i.e., $a_p^N(\lambda) = a_p(\lambda)/a_p(412)$). Then the extrapolation can be performed using the retrieved $[a_{CDOM}/a_t](412)$, and known S and $a_p^N(\lambda)$ as

$$\frac{a_{CDOM}}{a_t}(\lambda) = \frac{f \exp^{[S(412-\lambda)]}}{f \exp^{[S(412-\lambda)]} + \{1-f\} a_p^N(\lambda)}, \qquad \text{(A1)}$$

where $f = [a_{CDOM}/a_t](412)$.

[42] Here various values for S and $a_p^N(\lambda)$ were chosen on the basis of observed variability in CDOM and particulate

absorption spectra in marine waters. Values of 0.015, 0.020 and 0.025 nm^{-1} were adopted for S, which covers almost the whole range observed in marine waters [*Blough and Del Vecchio*, 2002; *Babin et al.*, 2003b]. For $a_p^N(\lambda)$, we used an averaged spectrum made out of the 99 $a_p(\lambda)$ spectra normalized to the value at 412 nm measured in the surface waters during the CASES field campaign. Except for a few number of spectra where the presence of phytoplankton pigments was dominant (with a $a_p(\lambda)$ peak at ~440 nm), most spectra approximately follow an exponential increase toward shorter wavelengths, which indicates the dominance of the a_{NAP} in the total particulate matter absorption (62 ± 18% at 443 nm). In addition to the average $a_p^N(\lambda)$ spectrum, two other spectra corresponding to the average ± 1.96*σ (i.e., a 95% confidence interval) were chosen to represent the limits of the a_p spectrum for low and high spectral dependency, respectively (Figure 7). The spectra for $a_p^N(\lambda)$ and $a_{CDOM}(\lambda)$, and an example of nine resulting $[a_{CDOM}/a_t]$ spectra for a given value of $[a_{CDOM}/a_t](412)$ are shown in Figure 7. Figure A1 shows an example of spectral DIC photoproduction (equation (6a)) obtained using two different AQYs (Figure 6) and various $[a_{CDOM}/a_t](\lambda)$.

Notation

λ	light wavelength (nm).
$a_x(\lambda)$,	absorption, scattering and attenuation
$b_x(\lambda)$,	coefficients for constituent x
$c_x(\lambda)$	respectively (m^{-1}). subscript x is either m (measured by ac-9), t (total), w (water), t-w (non-water constituents), $CDOM$ (chromophoric dissolved organic matter), p (particles), NAP (nonalgal particles), CDM (colored detrital material) or ϕ (phytoplankton).
$E_s(\lambda)$	downwelling irradiance just above the sea surface (W m^{-2} nm^{-1}).
$E_d(\lambda,z)$	downwelling irradiance at depth z (W m^{-2} nm^{-1} or mol photon m^{-2} s^{-1} nm^{-1}).
$L_u(\lambda,z)$	upwelling radiance at depth z (W m^{-2} nm^{-1} sr^{-1}).
$L_w(\lambda)$	water_leaving radiance (W m^{-2} nm^{-1} sr^{-1}).
$R_{rs}(\lambda)$	remote sensing reflectance above the sea surface (nm^{-1} sr^{-1}).
$AQY_x(\lambda)$	a quantum yield for the photoproduct x (mol x (mol photon)$^{-1}$ nm^{-1}).
P_x	spectrally depth-integrated production of photoproduct x (g x m^{-2} d^{-1}).

[43] **Acknowledgments.** This study was made possible by financial support from the Natural Sciences and Engineering Research Council of Canada (NSERC), the Fonds France Canada pour la Recherche (FFCR) (to MB), the Indian and Northern Affairs Canada (INAC) (to S.B.), the Department of Fisheries and Oceans Canada and the Canadian Space Agency (to P.L.), and the French Centre National de la Recherche Scientifique (PNTS program; to M.B.). S. Bélanger received a doctoral fellowship from the Fonds Québécois pour la Recherche sur la Nature et les Technologies (FQRNT). We are grateful to H. Xie and D. Siegel for their constructive comments on the manuscript. We are grateful to F. Fell, M. Ferrari, V. Fournier-Sicre, and G. Obolensky for then contribution to the collection and processing of the COAS/OOC data. We appreciated the contribution of S. Cizmeli to CASES field measurements and M. Twardowski for his assistance in the ac-9 data processing. We thank the crew of the CCGS *Amundsen* for their enthusiastic help onboard the ship. This is a contribution to the Canadian Arctic Shelf Exchange Study (CASES) under the overall direction of L. Fortier.

References

Arctic Climate Impact Assessment (2005), *Arctic Climate Impact Assessment: Scientific Report*, 1042 pp., Cambridge Univ. Press, New York.

Babin, M., A. Morel, V. Fournier-Sicre, F. Fell, and D. Stramski (2003a), Light scattering properties of marine particles in coastal and open ocean waters as related to the particle mass concentration, *Limnol. Oceanogr.*, *48*(2), 843–859.

Babin, M., D. Stramski, G. M. Ferrari, H. Claustre, A. Bricaud, G. Obolensky, and N. Hoepffner (2003b), Variations in the light absorption coefficients of phytoplankton, nonalgal particles, and dissolved organic matter in coastal waters around Europe, *J. Geophys. Res.*, *108*(C7), 3211, doi:10.1029/2001JC000882.

Bélanger, S. (2006), Response of light-related carbon fluxes in the Arctic Ocean to climate change: Quantification and monitoring of dissolved organic matter photo-oxidation in the Beaufort Sea using satellite remote sensing, Ph.D. thesis, 243 pp., Univ. Pierre et Marie Curie, Paris.

Bélanger, S., H. Xie, N. Krotkov, P. Larouche, W. F. Vincent, and M. Babin (2006), Photomineralization of terrigenous dissolved organic matter in Arctic coastal waters from 1979 to 2003: Interannual variability and implications of climate change, *Global Biogeochem. Cycles*, *20*, GB4005, doi:10.1029/2006GB002708.

Blough, N. V., and Del R. Vecchio (2002), Chromophoric DOM in the coastal environment, in *Biogeochemistry of Marine Dissolved Organic Matter*, edited by D. A. Hansell and C. A. Carlson, pp. 509–546, Academic Press, San Diego, Calif.

Bricaud, A., A. Morel, and L. Prieur (1981), Absorption by dissolved organic matter of the sea (yellow substance) in the UV and visible domains, *Limnol. Oceanogr.*, *26*(1), 43–53.

Carder, S. Hawes, K. Baker, R. Smith, R. Steward, and B. Mitchell (1991), Reflectance model for quantifying chlorophyll a in the presence of productivity degradation products, *J. Geophys. Res.*, *96*(C11), 20,599–20,611.

Cullen, J. J., R. F. Davis, J. S. Barlett, and W. L. Miller (1997), Toward remote sensing of UV attenuation, photochemical fluxes, and biological effects of UV in surface waters, paper presented at Current and Emerging Issues in Aquatic Science: Aquatic Science Meeting, Am. Soc. of Limnol. and Oceanogr., Santa Fe, N. M.

Defoin-Platel, M., and M. Chami (2007), How ambiguous is the inverse problem of ocean color in coastal waters?, *J. Geophys. Res.*, *112*, C03004, doi:10.1029/2006JC003847.

Del Vecchio, R., and A. Subramaniam (2004), Influence of the Amazon River on surface optical properties of the western tropical North Atlantic Ocean, *J. Geophys. Res.*, *109*, C11001, doi:10.1029/2004JC002503.

Gallegos, C. L., and P. J. Neale (2002), Partitioning spectral absorption in case 2 waters: Discrimination of dissolved and particulates components, *Appl. Opt.*, *41*, 4220–4233.

Garver, D. L., and D. A. Siegel (1997), Inherent optical property inversion of ocean color spectra and its biogeochemical interpretation: 1. Time series from the Sargasso Sea, *J. Geophys. Res.*, *102*(C8), 18,607–18,625.

Gordon, H. R. (1992), Diffuse reflectance of the ocean: Influence of nonuniform phytoplankton pigment profile, *Appl. Opt.*, *31*, 2116–2129.

Gordon, H. R., and K. Ding (1992), Self-shading of in-water optical instruments, *Limnol. Oceanogr.*, *37*(3), 491–500.

Harding, L. W., A. Magnuson, and M. E. Mallonee (2005), SeaWiFS retrievals of chlorophyll in Chesapeake Bay and the mid-Atlantic bight, *Estuarine Coastal Shelf Sci.*, *62*, 75–94.

Johannessen, S. C., W. L. Miller, and J. J. Cullen (2003), Calculation of UV attenuation and colored dissolved organic matter absorption spectra from measurements of ocean color, *J. Geophys. Res.*, *108*(C9), 3301, doi:10.1029/2000JC000514.

Keith, D. J., J. A. Yoder, and S. A. Freeman (2002), Spatial and temporal distribution of coloured dissolved organic matter (CDOM) in Narragansett Bay, Rhode Island: Implications for phytoplankton in coastal waters, *Estuarine Coastal Shelf Sci.*, *55*, 705–717.

Kishino, M., M. Takahashi, N. Okami, and S. Ichimura (1985), Estimation of the spectral absorption coefficients of phytoplankton in the sea, *Bull. Mar. Sci.*, *37*(2), 634–642.

Laurion, I., F. Blouin, and S. Roy (2003), The quantitative filter technique for measuring phytoplankton absorption: Interference by MAAs in the UV waveband, *Limnol. Oceanogr. Methods*, *1*(1), 1–9.

Lee, Z.-P. (Ed.) (2006), Remote sensing of inherent optical properties: Fundamentals, tests of algorithms, and applications, *Rep. 5*, 126 pp., Int. Ocean-Colour Coord. Group,Dartmouth, N.S., Canada.

Lee, Z. P., and C. M. Hu (2006), Global distribution of Case-1 waters: An analysis from SeaWiFS measurements, *Remote Sens. Environ.*, *101*, 270–276.

Lee, Z. P., K. L. Carder, T. G. Peacock, C. O. Davis, and J. L. Mueller (1996), Method to derive ocean absorption coefficients from remote-sensing reflectance, *Appl. Opt.*, *35*, 453–462.

Loisel, H., and A. Morel (2001), Non-isotropy of the upward radiance field in typical coastal (Case 2) waters, *Int. J. Remote Sens.*, *22*(2/3), 275–295.

Macdonald, R. W., et al. (1998), A sediment and organic carbon budget for the Canadian Beaufort Shelf, *Mar. Geol.*, *144*, 255–273.

Madronich, S., and S. Flocke (1999), The role of solar radiation in atmospheric chemistry, in *Handbook of Environmental Chemistry*, edited by P. Boule, pp. 1–26, Springer, Heidelberg, Germany.

McKee, D., A. Cunningham, and K. J. Jones (2002), Optical and hydrographic consequences of freshwater run-off during spring phytoplankton growth in a Scottish fjord, *J. Plankton Res.*, *24*(11), 1163–1171.

Mobley, C. D. (1999), Estimation of the remote-sensing reflectances from above-water measurements, *Appl. Opt.*, *38*, 7442–7455.

Mopper, K., and D. J. Keiber (2002), Photochemistry and the cycling of carbon, sulfur, nitrogen and phosphorus, in *Biogeochemistry of Marine Dissolved Organic Matter*, edited by D. A. Hansell and C. A. Carlson, pp. 455–507, Academic Press, San Diego, Calif.

Morel, A., and S. Bélanger (2006), Improved detection of turbid waters from ocean color sensors information, *Remote Sens. Environ.*, *102*, 237–249.

Morel, A., and L. Prieur (1977), Analysis of variations in ocean color, *Limnol. Oceanogr.*, *22*(4), 709–722.

Morel, A., et al. (2007), Optical properties of the clearest natural waters, *Limnol. Oceanogr.*, *52*(1), 217–229.

Morrison, J. R., and N. B. Nelson (2004), Seasonal cycle of phytoplankton UV absorption at Bermuda Atlantic Time-series Study (BATS) site, *Limnol. Oceanogr.*, *49*(1), 215–224.

Mueller, J. L., et al. (2003), Radiometric measurements and data analysis protocols, in *Ocean Optics Protocols for Satellite Ocean Color Sensor Validation*, rev. 4, vol. III, *NASA Tech. Memo., 21621*, 78 pp.

Nelson, N. B., and D. A. Siegel (2002), Chromophoric DOM in Open Ocean, in *Biogeochemistry of Marine Dissolved Organic Matter*, edited by D. A. Hansell and C. A. Carlson, pp. 547–578, Academic Press, San Diego, Calif.

Nelson, N. B., et al. (2007), Hydrography of chromophoric dissolved organic matter in the North Atlantic, *Deep Sea Res., Part I*, *54*, 710–731.

Pope, R. M., and E. S. Fry (1997), Absorption spectrum (380-700 nm) of pure water. II. Integrating cavity measurements, *Appl. Opt.*, *36*, 8710–8723.

Rachold, V., et al. (2004), Modern terrigenous organic carbon input to the Arctic Ocean, in *The Organic Carbon Cycle in the Arctic Ocean*, edited by R. Stein and R. W. MacDonald, pp. 33–41, Springer, Berlin.

Roesler, C. S., and M. J. Perry (1995), In situ phytoplankton absorption, fluorescence emission, and particulate backscattering spectra determined from reflectance, *J. Geophys. Res.*, *100*(C7), 13,279–13,294.

Roesler, C. S., M. J. Perry, and K. L. Carder (1989), Modeling in situ phytoplankton absorption from total absorption spectra in productive inland marine waters, *Limnol. Oceanogr.*, *34*, 1510–1523.

Ruddick, K. G., F. Ovidio, and M. Rijkeboer (2000), Atmospheric correction of SeaWiFS imagery for turbid coastal and inland waters, *Appl. Opt.*, *39*, 897–912.

Ruddick, K. G., V. De Cauwer, Y.-J. Park, and G. Moore (2006), Seaborne measurements of near infrared water-leaving reflectance: The similarity spectrum for turbid waters, *Limnol. Oceanogr.*, *51*, 1167–1179.

Sathyendranath, S., L. Prieur, and A. Morel (1989), A three-component model of ocean colour and its application to remote sensing of phytoplankton pigments in coastal waters, *Int. J. Remote Sens.*, *10*(8), 1373–1394.

Siegel, D. A., S. Maritorena, N. B. Nelson, and D. A. Hansell (2002), Global distribution and dynamics of colored dissolved and detrital organic materials, *J. Geophys. Res.*, *107*(C12), 3228, doi:10.1029/2001JC000965.

Sosik, H. (1999), Storage of marine particulate samples for light-absorption measurements, *Limnol. Oceanogr.*, *44*, 1139–1141.

Tassan, S., and G. M. Ferrari (1995), An alternative approach to absorption measurements of aquatic particles retained on filters, *Limnol. Oceanogr.*, *40*, 1358–1368.

Tassan, S., and G. M. Ferrari (2002), A sensitivity analysis of the 'transmittance-reflectance' method for measuring light absorption by aquatic particles, *J. Phytoplankton Res.*, *24*(8), 757–776.

Werdell, P. J., and S. W. Bailey (2005),.An improved in-situ bio-optical data set for ocean color algorithm development and satellite product validation, *Remote Sens. Environ.*, *98*, 122–140.

Zafiriou, O. C., S. S. Andrews, and W. Wang (2003), Concordant estimates of oceanic carbon monoxide source and sink processes in the Pacific yield a balance global "blue-water" CO budget, *Global Biogeochem. Cycles*, *17*(1), 1015, doi:10.1029/2001GB001638.

Zaneveld, J. R. V., J. C. Kitchen, and C. Moore (1994), The scattering error correction of reflecting-tube absorption meters, *Proc. SPIE Soc. Opt. Eng.*, *2258*, 44–55.

Zibordi, G., and G. M. Ferrari (1995), Instrument self-shading in underwater optical measurements—Experimental data, *Appl. Opt.*, *34*, 2750–2754.

M. Babin, Laboratoire d'Océanographie de Villefranche, Centre National de la Recherche Scientifique, Université Pierre et Marie Curie, F-06230 Villefranche-sur-Mer, France.

S. Bélanger, Département de Biologie, Chimie et Géographie, Université du Québec à Rimouski, 300 allée des Ursulines, Rimouski, QC, Canada G5L 3A1. (simon_belanger@uqar.qc.ca)

P. Larouche, Institut Maurice-Lamontagne, Pêches et Océans Canada, Mont-Joli, QC, Canada G5H 3Z4.